Title

Dynamic brain connectivity is a better predictor of PTSD than static connectivity

Journal

Human Brain Mapping, 38(9)

ISSN

1065-9471

Authors

Jin, Changfeng
Jia, Hao
Lanka, Pradyumna
et al.

Publication Date

2017-09-01

DOI

10.1002/hbm.23676

Peer reviewed

◆ Human Brain Mapping 38:4479–4496 (2017) ◆

Dynamic Brain Connectivity Is a Better Predictor of PTSD than Static Connectivity

Changfeng Jin,[1] Hao Jia,[2,3] Pradyumna Lanka,[2] D Rangaprakash ,[2,4] Lingjiang Li,[1] Tianming Liu,[5] Xiaoping Hu,[6] and Gopikrishna Deshpande [2,7,8]*

[1]*The Mental Health Institute, The Second Xiangya Hospital, Central South University, Changsha, China*
[2]*AU MRI Research Center, Department of Electrical and Computer Engineering, Auburn University, Auburn, Alabama*
[3]*Department of Automation, College of Information Engineering, Taiyuan University of Technology, Taiyuan, Shanxi, China*
[4]*Department of Psychiatry and Biobehavioral Sciences, University of California Los Angeles, Los Angeles, California*
[5]*Cortical Architecture Imaging and Discovery Lab, Department of Computer Science and Bioimaging Research Center, University of Georgia, Athens, Georgia*
[6]*Center for Advanced Neuroimaging, Department of Bioengineering, University of California, Riverside, California*
[7]*Department of Psychology, Auburn University, Auburn, Alabama*
[8]*Alabama Advanced Imaging Consortium, Auburn University and University of Alabama Birmingham, Alabama*

Abstract: Using resting-state functional magnetic resonance imaging, we test the hypothesis that subjects with post-traumatic stress disorder (PTSD) are characterized by reduced temporal variability of brain connectivity compared to matched healthy controls. Specifically, we test whether PTSD is characterized by elevated static connectivity, coupled with decreased temporal variability of those connections, with the latter providing greater sensitivity toward the pathology than the former. Static functional connectivity (FC; nondirectional zero-lag correlation) and static effective connectivity (EC; directional time-lagged relationships) were obtained over the entire brain using conventional models. Dynamic FC and dynamic EC were estimated by letting the conventional models to vary as a function of time. Statistical separation and discriminability of these metrics between the groups and their ability to accurately predict the diagnostic label of a novel subject were ascertained using separate support vector machine classifiers. Our findings support our hypothesis that PTSD subjects have stronger static connectivity, but reduced temporal variability of connectivity. Further, machine learning classification accuracy obtained with dynamic FC and dynamic EC was significantly higher than that obtained with

Additional Supporting Information may be found in the online version of this article.

Changfeng Jin, Hao Jia, and Pradyumna Lanka contributed equally to this work.

Conflicts of Interests: None of the authors report any conflicts of interests.

*Correspondence to: Gopikrishna Deshpande, AU MRI research center, Department of Electrical and Computer Engineering, Auburn University, Auburn, AL 36832. E-mail: gopi@auburn.edu

Received for publication 22 February 2017; Accepted 23 May 2017.

DOI: 10.1002/hbm.23676

Published online 12 June 2017 in Wiley Online Library (wileyonlinelibrary.com).

static FC and static EC, respectively. Furthermore, results also indicate that the ease with which brain regions engage or disengage with other regions may be more sensitive to underlying pathology than the strength with which they are engaged. Future studies must examine whether this is true only in the case of PTSD or is a general organizing principle in the human brain. *Hum Brain Mapp 38:4479–4496, 2017.*

Key words: resting-state functional magnetic resonance imaging; dynamic brain connectivity; functional connectivity; effective connectivity; post-traumatic stress disorder; support vector machine

INTRODUCTION

The view that the human brain works as a structurally connected and functionally integrated entity has been widely appreciated for decades [Deshpande and Hu, 2012; Deshpande et al., 2011; Friston, 1994; Friston et al., 1993; Greicius et al., 2009; Guye et al., 2010; Kaminski et al., 2001; Patel et al., 2006; Roebroeck and Daunizeau, 2011; Rogers et al., 2010; Stephan and Roebroeck, 2012; Valdes-Sosa et al., 2011]. With the advent of functional magnetic resonance imaging (fMRI) and technical advances in characterizing connectivity from fMRI data, functional aspects of connectivity in brain networks has received considerable attention. Functional connectivity (FC) specifically refers to measures of instantaneous (zero-lag, nondirectional) correlation between pairs of fMRI time series obtained from different brain regions, while effective connectivity (EC) measures the causal (time-lagged, directional) relationships between them. It is noteworthy that both FC- and EC-based methods characterize connectivity in the brain that is of functional origin.

Previous studies have mainly investigated FC and EC over a network of brain regions based on the assumption that connectivity was stationary over time. Even though this assumption simplified the analysis procedure, there is recent evidence to suggest that it may not be true [Chang and Glover, 2010]. To address this issue, many recent works have explored the dynamics of brain connectivity from resting-state fMRI. Most of them investigated dynamic FC using sliding windows [Chang et al., 2013a, 2013b; Cribben et al., 2012; Deshpande et al., 2006; Keilholz et al., 2013; Leonardi et al., 2013; Majeed et al., 2011]. In particular, Handwerker et al. conducted a sliding window analysis on dynamic FC mainly in the frequency domain [2012], Lee et al. explored sliding windowed dynamic FC at different frequency bands using high sampling rate achieved through MR-encephalography [2013], and Chang and Glover explored dynamic FC by using wavelet-based time-frequency analysis [2010]. In addition, observations from electrophysiological studies using EEG [Dimitriadis et al., 2012] and simultaneous EEG/fMRI [Britz et al., 2010; Chang et al., 2013a,b; Tagliazucchi et al., 2012] have demonstrated the existence of temporal variations in FC derived from resting-state fMRI and their electrophysiological correlates. Hutchison et al. [2012] showed that resting-state functional connectivity can exhibit nonstationary and spontaneous relationships regardless of conscious, cognitive processing, while Jia et al. showed that dynamic variations in FC are behaviorally relevant [2014]. For a comprehensive overview of dynamic FC of resting-state fMRI, please refer to the paper by Hutchison et al. [2013].

Conversely, there have been few studies exploring dynamic EC in brain networks. For example, Havlicek et al. proposed an approach to estimate dynamic Granger causality in the frequency domain [2010], while Sato et al. [2006], Lacey et al. [2011], and Kapogiannis et al. [2014] used wavelet extension of Granger causality to investigate dynamic EC in the time domain. Both studies were illustrated with application to task-based fMRI. Other studies have applied dynamic EC to task-based fMRI as well [Feng et al., 2015; Grant et al., 2014, 2015; Hampstead et al., 2016; Hutcheson et al., 2015; Libero et al., 2015; Wheelock et al., 2014].

The studies discussed above raise the possibility that conventional static measures of connectivity smear dynamic information in brain networks, since only one connectivity value is obtained for the entire length of the scan, potentially leading to loss of information and sensitivity to the underlying neuronal processes. While there is evidence to believe that nonstationary dynamics exists in brain networks obtained from resting-state fMRI, it is yet unclear whether such dynamics provide any additional sensitivity to the underlying neuronal processes, especially in clinical diagnostic applications. A recent report showed that dynamic FC is related to real-world cognitive behaviors [Thompson et al., 2013]. Further, recent works have shown that dynamic connectivity signatures in healthy subjects are different from that in subjects diagnosed with mental disorders such as post-traumatic stress disorder (PTSD) [Li et al., 2014] and schizophrenia [Sakoğlu et al., 2010]. However, the above studies do not answer the key question of whether dynamic connectivity provides any additional sensitivity to underlying neuronal processes than what is provided by conventional static connectivity.

Hyper-connectivity is considered a response to neurological disruption [Hillary et al., 2015], which is observed in psychiatric disorders like PTSD [Cisler et al., 2014; Hayes et al., 2012; Simmons and Matthews, 2012]. Reduced temporal variability of connectivity is considered to be associated with psychiatric disorders [Sakoğlu et al., 2010],

and compromised behavioral performance in healthy persons [Jia et al., 2014]. This reduced variability of connectivity could be a result of compromised ability to dynamically adjust behaviors and thoughts to changing conditions. Such reduced variability in function is widely recognized in other bodily systems, for example, reduced heart rate variability is considered a risk factor of cardiovascular disease [Greiser et al., 2009]. Internal body/mental states as well as external environmental influences are continually changing, hence a healthy system is expected to modify its function in real-time to accommodate such changes. In such terms, a temporally "frozen" connectivity reflects compromised brain health. Motivated by these observations, we propose that the ability of brain regions to engage and disengage from other brain regions provides a characterization which is fundamentally different from that obtained from conventional static connectivity. Consequently, we hypothesize that the healthy brain is characterized by greater temporal variability of corresponding brain connections as compared to unhealthy brains in general. We specifically test this hypothesis in the case of PTSD, wherein we postulate that the brains of persons with PTSD is characterized by elevated static connectivity (as found in previous reports [Cisler et al., 2014]), coupled with decreased temporal variability of those connections, leading to a situation wherein hyper-connected brain regions do not disengage effectively enough. Further, we hypothesize that dynamic FC and EC will provide higher sensitivity in discriminating PTSD from healthy controls than that provided by their static counterparts.

We tested the above hypotheses by estimating both dynamic FC (DFC) and dynamic EC (DEC) in addition to the conventional static measures, static FC (SFC) and static EC (SEC), from resting-state fMRI data. For obtaining DFC, we employed moving-windowed Pearson's correlation with window length being determined adaptively by the augmented Dickey–fuller unit root test (ADF test) [Jia et al., 2014]. SFC was estimated using Pearson's correlation between the entire time series. For obtaining DEC, we employed dynamic Granger causality (DGC) while correlation-purged Granger causality (CPGC) [Deshpande et al., 2010b] was used as the static EC (SEC) measure. These measures were estimated from mean resting-state time series extracted from 190 functionally homogeneous regions across the entire brain [Craddock et al., 2012].

PTSD is a psychiatric disorder which is associated with exposure to traumatic events that have a profound impact, resulting in symptoms like re-experiencing of the event or flashback, avoidance/numbing/depression, hyper-arousal, along with dissociative symptoms [American Psychiatric Association, 1994; Yehuda, 2002]. The pathogenesis of PTSD yet remains unclear. FMRI studies have provided useful characterization of PTSD, although many of them are task-related and hence difficult for subjects to perform with similar accuracy as healthy controls [Jatzko et al., 2006; Whalley et al., 2013]. Recent studies have increasingly explored the use of resting-state fMRI [Qin et al., 2012; Yin et al., 2011, 2012] given the ease of acquiring such data from patient populations, and lack of requirements such as matching task performance with a control group. Most connectivity studies on PTSD have focused on static FC, while ignoring the dynamic variation of connectivity over time [Simmons and Matthews, 2012]. Dynamic FC is related to real-world cognitive behaviors [Thompson et al., 2013], which renders it to be a suitable tool for studying disorders like PTSD where cognitive functioning is compromised. Additionally, there have been no effective connectivity studies (either static or dynamic) on PTSD to date. Hence, the study of PTSD using the aforementioned techniques is relevant.

To test whether dynamic connectivity measures provide higher sensitivity to the underlying neuronal processes which are altered in PTSD, we used each of the following measures—SFC, SEC, variance of DFC, and variance of DEC—as features in four separate support vector machine (SVM) classifiers to estimate the accuracy with which they were able to predict the diagnosis of a novel subject. We also evaluate whether using a time-varying window length instead of a fixed window length for calculation of DFC is more sensitive to the dynamic changes in neural activity by providing a better measure of the fluctuations in connectivity, leading to an improvement in the classification accuracy.

MATERIALS AND METHODS

Subjects

Participants with PTSD and matched healthy controls (all right handed) were recruited after the 2008 Wenchuan earthquake, Sichuan, China. The data came from 99 runs from 76 trauma-exposed healthy adult subjects, and 146 runs from 73 adult PTSD subjects, with some subjects scanned twice. Informed consent was obtained from all subjects after they understood detailed information about the study protocol, which was approved by the IRB of the Second Xiangya Hospital and the Central South University, Changsha, China. Controls were matched in terms of gender and age (within 2 years), as well as education (within 5 years).

Data Acquisition and Preprocessing

All subjects in the scanner were instructed to keep their eyes closed, relax, and not focus on any particular thoughts. T2*-weighted echo planar functional images were acquired in a 3T MRI scanner (EXCITE; General Electric). The acquisition parameters were: 200 volumes per scan, In-plane matrix of 64×64 (voxels), 30 axial slices, field of view (FOV) = 220×220 mm^2, flip angle (FA) = 90°, TR (repetition time)/TE (echo time) = 2,000 ms/30 ms, slice thickness 4 mm with 1 mm gap. Preprocessing of

data was accomplished using Data Processing Assistant for Resting-State fMRI software (DPARSF) [Yan and Zang, 2010], and included slice timing correction, rigid body registration, detrending, and regressing out of white matter (WM) and cerebrospinal fluid (CSF) signals as well as six motion parameters, normalization to MNI template with 2 × 2 × 2 mm^3 resolution, spatial smoothing with 4 × 4 × 4 mm^3 Gaussian kernel and finally 0.01–0.1 Hz temporal band pass filtering. 190 functionally homogeneous brain regions derived from spectral clustering of resting-state fMRI data were identified from the CC200 brain atlas [Craddock et al., 2012]. Mean time series from each of the 190 regions were extracted from the preprocessed data from each subject and input into the connectivity models described below.

Static and Dynamic Effective Connectivity

Effective connectivity refers to the directional influence of one brain region over another. Various methods exist for characterizing EC in brain networks. They can be classified mainly into model-based methods requiring a priori assumptions about the underlying connectional architecture such as dynamic causal modeling (DCM) [Friston et al., 2003] and structural equation modeling (SEM) [McIntosh and Gozales-Lima, 1994], and data-driven methods such as Granger causality [Geweke, 1982; Granger, 1969]. Since we used 190 regions covering the entire brain, no assumptions could be made about the underlying connectional architecture. Further, model-based methods become computationally intractable when the number of ROIs increases [Lohmann et al., 2012]. Considering these factors, we adopted Granger causality for investigating whole brain EC.

Granger causality is based on the principle that if the past of one time series helps predict the present and future of another time series, then there must be a causal influence from the former time series to the latter. Given k time series $\boldsymbol{Y}(t) = [x_1(t)\ x_2(t)\ \ldots\ x_k(t)]$, with k being 190 in this study, we can construct matrices $\boldsymbol{X}(t) = = [x_i(t)\ x_j(t)]$, where $i,j = 1 \ldots 190$, which represent all pairwise combinations of time series. We can then define bivariate vector autoregressive (BVAR) model with model parameters $\boldsymbol{A}(n)$ of order p is given by:

$$\boldsymbol{X}(t) = \boldsymbol{V} + \sum_{n=1}^{p} \boldsymbol{A}(n)\boldsymbol{X}(t-n) + \boldsymbol{E}(t) \quad (1)$$

Where $\boldsymbol{V}$ is the intercept vector representing nonzero mean component, n is the time lag, and $\boldsymbol{E}(t)$ is the vector corresponding to the residuals. In our scenario, time series was detrended so that $\boldsymbol{V} = 0$. Direct causal influences among the k time series can be inferred from the BVAR coefficients as follows.

$$D_{ij} = \sum_{n=1}^{p} a_{ij}^2(n) \quad (2)$$

Where each a_{ij}, $i, j = 1{:}k$, is one element of matrix $\boldsymbol{A}$. The effects of instantaneous correlation is modeled as the zero-lag terms and introduced into the modified BVAR model as below [Deshpande et al., 2010b].

$$\boldsymbol{X}(t) = \boldsymbol{V} + \sum_{n=0}^{p} \boldsymbol{A}'(n)\boldsymbol{X}(t-n) + \boldsymbol{E}'(t) \quad (3)$$

Where the diagonal elements of $\boldsymbol{A}'(0)$ are zeros such that only instantaneous cross-correlation, rather than zero-lag auto-correlation, are modeled. Accordingly, correlation-purged Granger causality (CPGC) [Deshpande et al., 2010b] is defined as:

$$CPGC_{ij} = \sum_{n=1}^{p} \left[a'_{ij}(n)\right]^2 \quad (4)$$

Where each a'_{ij} is one element of the matrix $\boldsymbol{A}'$. Note that $\boldsymbol{A}'(1) \ldots \boldsymbol{A}'(p) \neq \boldsymbol{A}(1) \ldots \boldsymbol{A}(p)$ and the $\boldsymbol{A}'(1) \ldots \boldsymbol{A}'(p)$ represent the causal influence which is purged of zero-lag correlation "leakage" effects as shown before [Deshpande et al., 2010b]. The order p of this modified BVAR is determined by Bayesian Information Criterion (BIC) [Schwartz, 1978]. CPGC values obtained from the entire time series represented SEC in this study. For methodological details and applications of Granger causality-based SEC to task-based and resting-state fMRI data, please refer to the following previous publications [Bressler and Seth, 2011, Deshpande et al., 2008, 2009, 2010a, 2011, 2013; Hampstead et al., 2011; Krueger et al., 2011; Liang et al., 2014, Pruesse et al., 2011; Roebroeck et al., 2005; Sathian et al., 2011; Stilla et al., 2007, 2008; Strenziok et al., 2011]. While most of these previous studies used a small number of ROIs, we had 190 ROIs. This makes it harder to accurately estimate the 190 × 190 coefficient matrix $\boldsymbol{A}'$ given that the length of each ROI time series was only 200 time points. Therefore, we evaluated the connectivity between ROIs in a pairwise fashion for SEC (as well as for DEC described below).

We adopted dynamic Granger causality method (DGC) for estimating DEC. The DGC model is the same as before [Eq. (3)] except that the coefficient matrix $\boldsymbol{A}$ is allowed to be a function of time. Accordingly, a temporally adaptive BVAR process analogous to Eq. (3) can be defined as

$$\boldsymbol{X}(t) = \boldsymbol{V}(t) + \sum_{n=1}^{p} \boldsymbol{A}(n,t)\boldsymbol{X}(t-n) + \boldsymbol{E}(t) \quad (5)$$

It is noteworthy that coefficient matrix $\boldsymbol{A}(n,t)$ is now a function of both lag n and time t, and can be estimated using a Kalman filter as shown before [Arnold et al., 1998]. Recent studies have used the dynamic BVAR model

in task-based fMRI connectivity studies [Sathian et al., 2013]. Analogous to Eq. (2), the DGC metric is then given by

$$DGC_{ij}(t) = \sum_{n=1}^{p} [a_{ij}(n,t)]^2 \quad (6)$$

The model order is determined by BIC as in the case of SEC. To make DGC smoothly change over time, the impact of DGC values in the recent past is taken into account for the calculation of the current DGC value by the Kalman filter. The degree of smoothness is controlled by the Kalman filter's forgetting factor *FF*. The *FF* is determined by minimizing the variance of the estimated model error energy [Havlicek et al., 2010; Schlogl et al., 2000].

$$FF = \arg\left\{\min\left(\mathrm{var}\left(\hat{\boldsymbol{E}}(t)^2\right)\right)\right\} \quad (7)$$

Where $\hat{\boldsymbol{E}}(t)$ is the estimate of $\boldsymbol{E}(t)$ and "var" is the variance operator. It was empirically observed that the Kalman filter estimated needed 10–15 time points to converge. Also considering the fact that initial time points in fMRI time series are routinely discarded to allow the MR signal to achieve T1 equilibration, the DGC values obtained from the first 20 time points were discarded.

Static and Dynamic Functional Connectivity

Functional connectivity is a measure of zero-lag, instantaneous synchronization of signals obtained from different brain regions and is commonly characterized by Pearson's correlation coefficient between ROI time series. Consequently, Pearson's correlation calculated over entire time series was adopted as the measure of conventional SFC. For the dynamic version of FC, we used windowed Pearson's correlation moving along the time axis. Most studies to date have used fixed sliding rectangular windows to calculate time-varying FC [Chang and Glover, 2010; Chang et al., 2013a,b; Cribben et al., 2012; Handwerker et al., 2012; Hutchison et al., 2012; Keilholz et al., 2013; Lee et al., 2013; Leonardi et al., 2013; Majeed et al., 2011]. Others have used sliding windows of other shape, such as Hamming window [Handwerker et al., 2012]. Given its simplicity, we have used rectangular windows in this work. For fixed-length sliding windows, the window length is a very important parameter which should be determined with enough caution, since different lengths would produce different smoothing effects [Chang and Glover, 2010; Leonardi et al., 2013]. For a comprehensive review of DFC, please see Hutchison et al. [2013]. In this work, we relaxed the restriction of fixed window length and used time-varying window lengths instead. There is no data to suggest that the minimum length of the window within which resting-state fMRI data is stationary, is constant over time. Fixed window lengths were used previously more for convenience than anything else. The principle we adopted is that the window length used must be the minimum length at which the time series become stationary, so that FC can be calculated over a period when the signal is stationary. The minimum window length condition allows us to capture maximum available dynamics. To guarantee that the time series segment within the window under consideration is locally stationary, we employed the Augmented Dickey–Fuller test (ADF test) [Said and Dickey, 1984]. The details of this statistical test and its relevance to stationarity of a time-series is explained below.

Stationarity in the wide-sense is achieved when the first and second moments (viz. mean and variance) of the time-series remain the same. The Dickey–Fuller test [Dickey and Fuller, 1979] is based on the concept of the existence of a unit-root in the first-order AR model parameters for the time-series. The idea is explained here with an example. Let us take two processes:

1. $x(n) = 1*x(n\text{-}1) + e$ . . .has a unit root
2. $y(n) = 0.7*y(n\text{-}1) + e$ . . .does not have a unit root

In both the processes, the time-series is modeled as having its global mean equal to zero, the instantaneous mean represented by the AR parameter and its instantaneous variance represented by the error term.

Process-1: The instantaneous mean of every successive time point is same as that of the previous time point, hence, the model has no tendency to approach the global mean value of 0. It is possible that this process can go on for long runs without a zero-crossing, typical of nonstationarity.

Process-2: The instantaneous mean of every successive point is smaller than that of the previous point, hence, it always tends toward the global mean of 0. The process is constantly thrown away from the global mean by the effect of error (variance) term, however, its tendency to approach zero global mean will keep the process stationary.

The Augmented Dickey–Fuller (ADF) test is an extension of the Dickey–Fuller test for more complicated time series by expanding to include the time-lags, but the underlying concept remains the same. From this example, we can see that a given time series tends to be increasingly more stationary as the root of underlying AR process moves away from the value of 1 toward 0. The ADF test statistically tests for the presence of a unit root, and detects a nonstationarity when the null hypothesis (i.e., unit root exists) becomes true.

Our procedure for application of the ADF test and sliding of the window was as follows. At a given time point t_1, we chose the initial window length to be $m_{\text{-}}$ ($m_{\text{-}}$=10 TRs in our work), and did ADF test on time series within [t_1-$m_{\text{-}}$+1, t_1] from all 190 regions. If no unit root existed for all 190 time series, we assumed that they were consistently stationary and used these windowed time series to calculate Pearson's correlation and assigned that value to DFC at time point t_1. Otherwise, the window length was increased by one time point (1 TR) such that the windowed time series started

from t_1-m_- to t_1, and then we redid the ADF test. We iterated this procedure for t_1 until consistent stationarity was achieved or the maximum window length was reached, in which case we then moved on to the next time point t_1+1 and calculated the window length for t_1+1. Previous studies have used fixed sliding windows of lengths varying from 15 to 120 TRs and similar step size [Bassett et al., 2011; Chang and Glover, 2010; Handwerker et al., 2012; Hutchison et al., 2012; Leonardi et al., 2013]. The data used in this work had a relatively longer TR of 2 s, and hence we set the minimum window length to be 10 TRs (20 s) and maximum window length to be 50 TRs (100 s). The choice of minimum window length was motivated by the consideration that it must have sufficient sampling points to capture temporal dynamics of FC. Two factors influenced the choice of maximum window length. First, it had to be long enough to capture the slowest variations, but short enough so that it does not encompass a large portion of the relatively short time series of 200 TRs we had at our disposal. In order to balance these requirements, a maximum window length of 50 TRs was chosen which in our case could capture the fluctuations upto 0.01 Hz. We empirically observed that in a vast majority of cases, the window lengths calculated by the DF test was between these 10 and 50 TRs. However, it is noteworthy that if the time series were longer, it is possible to choose a longer maximum window length while performing the DF test. The first 50 data points of time series were preserved for performing the DF test of the first sliding window. Thus, t_1 started from the 50th time point and the dynamic FC had a length of 150 time points (200 is the total number of time points). To understand whether using a time-varying sliding window length aids in improving the classification accuracy, we decided to calculate DFC by using both a fixed window length (window length = 20 TR = 40 s) and the time-varying window length procedure described above.

RCE-SVM Classification

Here, we describe the method used to classify PTSD subjects and healthy control using dynamic and static connectivity metrics so that their ability to predict the diagnostic label of a novel subject can be assessed. As argued before, the predictive potency of neuroimaging markers obtained from such supervised learning models provide better assessments of their clinical utility compared to simple statistical separation determined by *t*-tests [Craddock et al., 2009; Deshpande et al., 2010c]. Eight separate classifiers were employed, with each one of them receiving one of the following metrics as features from all subjects as inputs: CPGC, Pearson's correlation, variance of DGC, variance of windowed Pearson's correlation with fixed window length, variance of windowed Pearson's correlation with time varying window length, mean of DGC, mean of windowed Pearson's correlation with a fixed window length, and finally the mean of windowed Pearson's correlation with time-varying window length. The variances of dynamic connectivity metrics were employed to capture information regarding the temporal variability of brain connectivities. For the effective connectivity measures (SEC, DEC), there were 190 (number of regions) $\times$ 189 (number of regions-1) = 35,910 features, while for the functional connectivity measures we have 190 (number of regions) *189 (number of regions-1)/2. = 17,955 features for every subject. To effectively reduce the number of features, we conducted a two sample *t*-test in order to determine those features which were significantly ($P < 0.05$) different between the two groups (PTSD and healthy controls). After this *t*-test filtering, the number of features reduced to around 2,000 (the precise number of features which were significantly different between the groups varied for different metrics). In order to make the classifier performances comparable, we selected the top 1,000 features with the lowest *p*-values and input those into the RCE- SVM [Deshpande et al., 2010c; Yousef et al., 2007] classifier.

The statistical separation of features obtained from a *t*-test does not guarantee the predictive power or generalizability of those features for inferring the diagnostic label of a novel subject, which can be provided by classifiers. Wide applicability of SVM as a machine learning approach [Vapnik, 1995] with successful applications in many different fields [Wang, 2005] motivated our choice of SVM for classification. More so, SVM has been the most popular classifier in neuroimaging applications [Craddock et al., 2009]. The recursive cluster elimination (RCE) algorithm is a "wrapper" method for feature selection, in which we used a soft margin, SVM (linear kernel, $C = 1$) wherein uninformative feature clusters are eliminated based on their contribution to classification accuracy obtained from SVM, and is considered to be more powerful than "filtering" methods such as *t*-test which pick the discriminative features a priori based on statistical separation [Inza et al., 2004; Pan, 2002]. However, we used *t*-test "filtering" to reduce the number of input features and then used the RCE "wrapper" approach on the remaining significant features in an effort to utilize the merits of both "filtering" and "wrapper" approaches. A schematic illustrating the RCE algorithm used for feature reduction using RCE-SVM is shown in Figure 1. Generally, the classification accuracy tends to increase as noninformative features are removed. However, sometimes throwing away clusters could lead to drop in accuracy because the features in the thrown cluster could be informative, but not as informative about the discriminability between the groups as the retained features. However, as a consequence of the algorithm, the average classification accuracy per each cluster always increases implying that a slight loss is accuracy is offset by a significant reduction in number of features, thereby improving the interpretability of the result and also making the accuracy obtained generalizable and less prone to over-fitting. The classification accuracy was obtained at each iteration and plotted. Also, the contribution of each

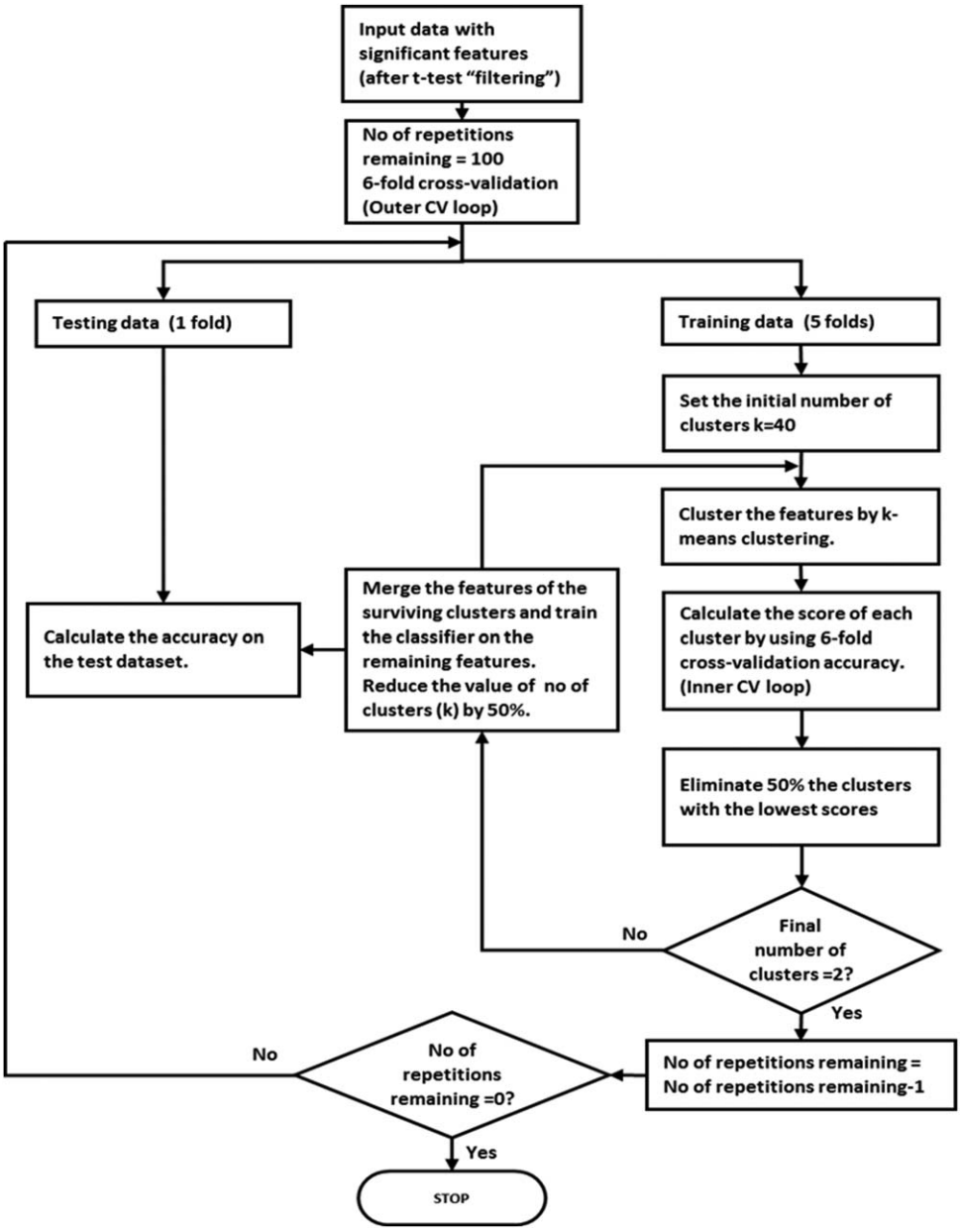

Figure 1.
Schematically illustrating the RCE-SVM algorithm.

feature toward obtaining highest classification accuracy was estimated and an SVM "score" was assigned to each feature. The features with the highest scores responsible for obtaining maximum accuracy were subsequently plotted. As shown in previous works, the RCE-SVM algorithm maintains full separation of training and testing data [Kriegeskorte et al., 2009] and hence avoids any bias in classification. Please refer to previous publications for complete details about the RCE-SVM algorithm [Deshpande et al., 2010c,; Yousef et al., 2007]. The RCE-SVM algorithm was implemented in MATLAB (Mathworks, Natick, USA). Using a *t*-test to identify the significant features is done on both the training data and the testing data before the reduced features are input into the RCE-SVM algorithm could lead to over-fitting. So, we also decided to identify only the top 1,000 significant features by *t*-test "filtering" only on the training data, and the significant features thus obtained are used for the testing data in the test step (this

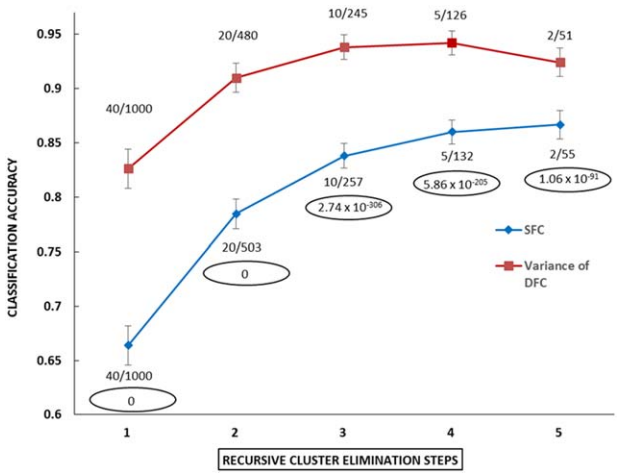

Figure 2.

Classification accuracy obtained from SFC and variance of DFC. *X*-axis represents recursive cluster elimination steps in RCE-SVM algorithm. Red line: classification accuracy obtained using variance of DFC. Blue line: classification accuracy obtained using SFC. The number pairs above/below each knot denote the number of feature-clusters remaining (first number) and the number of features remaining (second number) at every cluster elimination step. Numbers in circles represent the *p*-value obtained by doing a one-sided *t*-test comparing classification accuracy obtained by SFC with variance of DFC (alternative hypothesis: accuracy using variance of DFC > accuracy using SFC) at every cluster elimination step. The error bars indicate the standard deviation in classification accuracy. [Color figure can be viewed at wileyonlinelibrary.com]

modified classification procedure is shown in Fig. S1 in Supporting Information S1). This ensures that the results we get are an unbiased estimates of accuracy.

RESULTS

Figure 2 shows the mean classification accuracies obtained by SFC and DFC, while Figure 3 shows the mean classification accuracies obtained by SEC and DEC. It can be seen that, with each RCE step, uninformative features are eliminated and the remaining features are re-classified until we are left with only two feature clusters. The classification accuracy generally tends to increase until a point of inflection is reached for variance of DFC and DEC, which is at the fourth RCE step with only five feature-clusters remaining, at which the accuracy peaks at 94.2% and 90.9% for variance of DFC and DEC, respectively. Any further reduction in the number of clusters/features reduces the classification accuracy.

Removal of any more DFC and DEC features resulted in decreased accuracy indicating that those features were essential for peak accuracy. This was not the case for SFC and SEC, wherein the accuracy kept increasing until the final RCE step with peak accuracies of 86.7% and 88.2% for SFC and SEC, respectively.

It is noteworthy here that for both functional and effective connectivity measures, the variability of their dynamics had higher discriminatory power between the groups as compared to their conventional static counterparts. Digits in circles at every feature-cluster elimination step represent the *p*-value obtained by performing a one-tailed *t*-test comparing classification accuracy of DFC to SFC, and DEC to SEC. The alternative hypothesis for this *t*-test was that the accuracy of the variance of DFC/DEC is greater than that obtained by SFC/SEC, respectively. Figures 2 and 3 demonstrate that at each RCE step, the accuracies obtained by dynamic connectivity metrics are significantly greater than those obtained by static connectivity metrics.

The classification accuracy obtained by the variance of a time-varying adaptive window length DFC was significantly higher than that obtained by the variance of the DFC calculated by a sliding window of fixed window length (see Fig. 4). This implies that variance of DFC calculated by a time-varying window better captures the dynamic fluctuations of brain connectivity, thus giving a higher accuracy. We also explored the effect of sliding the window by 5 TR instead of 1 TR in the calculation of DFC.

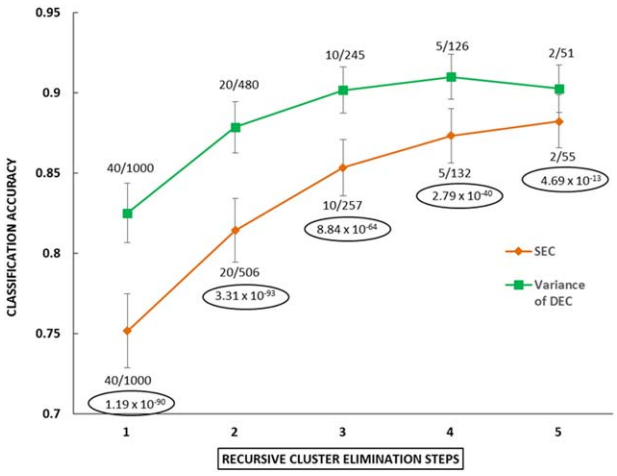

Figure 3.

Classification accuracy obtained from SEC and variance of DEC. *X*-axis represents recursive cluster elimination steps in RCE-SVM algorithm. Green line: classification accuracy obtained using variance of DEC. Orange line: classification accuracy obtained using SEC. The number pairs above/below each knot denote the number of feature-clusters remaining (first number) and the number of features remaining (second number) at every cluster elimination step. Numbers in circles represent the *p*-value obtained by doing a one-sided *t*-test comparing classification accuracy obtained by SEC with variance of DEC (alternative hypothesis: accuracy using variance of DEC > accuracy using SEC) at every cluster elimination step. The error bars indicate the standard deviation in classification accuracy. [Color figure can be viewed at wileyonlinelibrary.com]

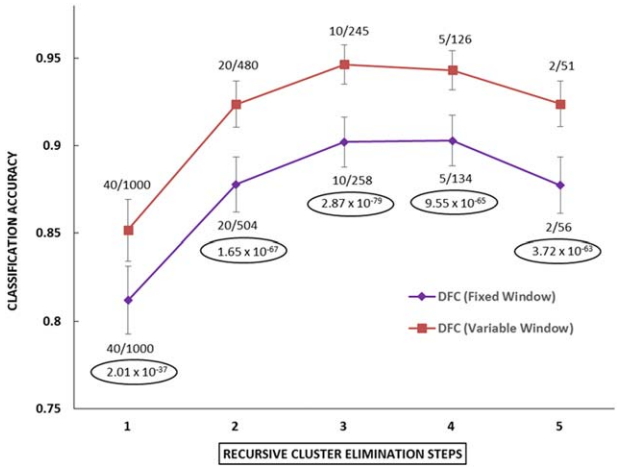

Figure 4.

Classification accuracy obtained from variance of fixed window DFC and variance of time-varying window DFC. *X*-axis represents recursive cluster elimination steps in RCE-SVM algorithm. Purple line: classification accuracy obtained using variance of DFC calculated by using a fixed window. Red line: classification accuracy obtained using variance of DFC calculated by using a time-varying window. The number pairs above/below each knot denote the number of feature-clusters remaining (first number) and the number of features remaining (second number) at every cluster elimination step. Numbers in circles represent the *p*-value obtained by doing a one-sided *t*-test comparing classification accuracy obtained by variance of DFC (Fixed window) with variance of DFC (variable window) (alternative hypothesis: accuracy using variance of DFC (variable window) $>$ DFC (Fixed window)) at every cluster elimination step. The error bars indicate the standard deviation in classification accuracy. [Color figure can be viewed at wileyonlinelibrary.com]

The corresponding results obtained from RCE-SVM classification procedure are shown in the Figures S8 and S9 in the Supporting Information S2 for both the original classification procedure (Fig. 1) and the modified classification procedure (Supporting Information Fig. S1), respectively. The results indicate that the classification accuracy obtained by sliding the window by 5 TR is very similar to the accuracy obtained by sliding the window by 1 TR.

In Figures 5 and 6, we compare the accuracies of SFC and the mean of DFC with time-varying and fixed window respectively. We found that the information encoded by the mean of DFC calculated by the fixed window length is similar to the information encoded by SFC as reflected by their classification accuracy. Also, the mean of DFC calculated by using a time-varying window length encodes more information about the state of the brain than the mean DFC measure obtained by fixed window length sliding window and Pearson's correlation coefficient. Similarly, we plot the accuracy obtained by mean of DGC and CPGC in Figure 7 which shows that the accuracy obtained by using mean of DGC is significantly higher than CPGC which implies that they represent different measures of directional neural activity.

Since the above results might be prone to over-fitting as discussed previously, in Figures S2, S3, S4, S5, S6, S7 in the Supporting Information, we plot the above results with the *t*-test "filtering" done only on the training data thereby leaving the testing data untouched. The above trends still hold true. Please refer to Supporting Information S1 for more information.

We identified the connectivity paths which exhibited significantly greater variance in connectivity in controls compared to PTSD for both the dynamic connectivity measures, DFC and DEC. A power spectrum density plot shown in Figures 8 and 9 was plotted by taking the above paths into consideration to identify the significant frequencies of fluctuations between the controls and PTSD subjects. The results indicate that the total power for the controls is higher than PTSD patients across all frequencies and the difference in power is statistically significant for both the connectivity measures (DFC and DEC). These results lend credence to the fact that, the engagement and disengagement of different brain regions across a broad

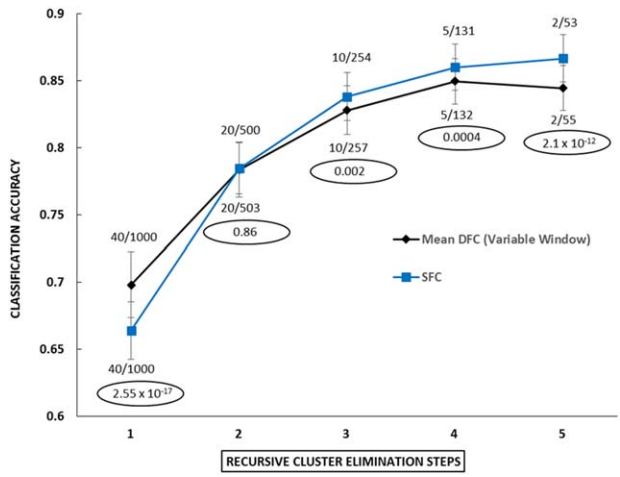

Figure 5.

Classification accuracy obtained from mean of variable window DFC and SFC. *X*-axis represents recursive cluster elimination steps in RCE-SVM algorithm. Black line: classification accuracy obtained by using mean of DFC calculated by using a variable window. Blue line: classification accuracy obtained using SFC. The number pairs above/below each knot denote the number of feature-clusters remaining (first number) and the number of features remaining (second number) at every cluster elimination step. Numbers in circles represent the *p*-value obtained by doing a two-sided *t*-test comparing classification accuracy obtained by mean of DFC (variable window) with SFC (alternative hypothesis: accuracy using mean of DFC (variable window) $\neq$ SFC) at every cluster elimination step. The error bars indicate the standard deviation in classification accuracy. [Color figure can be viewed at wileyonlinelibrary.com]

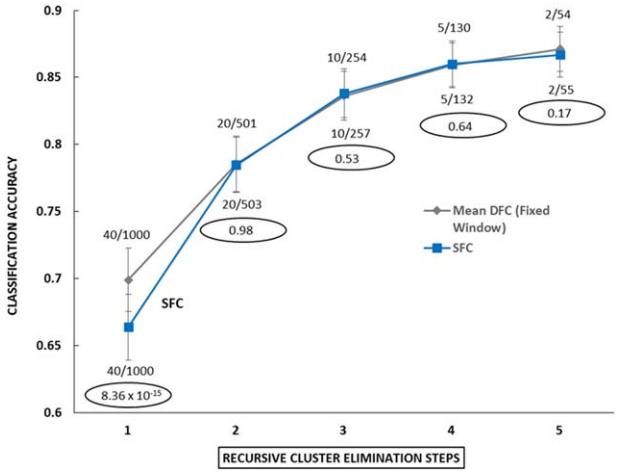

Figure 6.

Classification accuracy obtained from mean of fixed window DFC and SFC. *X*-axis represents recursive cluster elimination steps in RCE-SVM algorithm. Gray line: classification accuracy obtained by using mean of DFC calculated by using a fixed window. Blue line: classification accuracy obtained using SFC. The number pairs above/below each knot denote the number of feature-clusters remaining (first number) and the number of features remaining (second number) at every cluster elimination step. Numbers in circles represent the *p*-value obtained by doing a two-sided *t*-test comparing classification accuracy obtained by mean of DFC (fixed window) with SFC (alternative hypothesis: accuracy using mean of DFC (fixed window) ≠ SFC) at every cluster elimination step. The error bars indicate the standard deviation in classification accuracy. [Color figure can be viewed at wileyonlinelibrary.com]

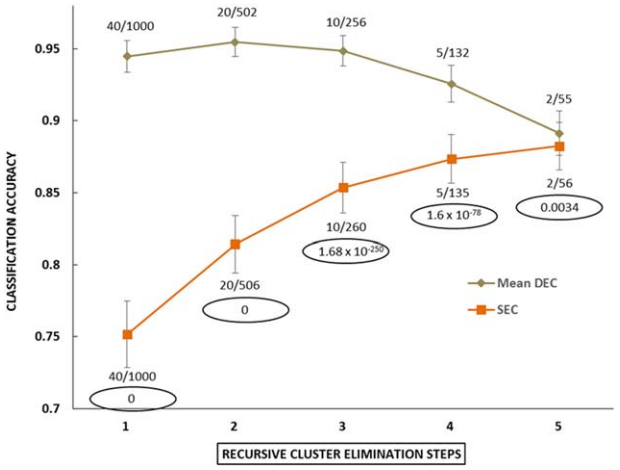

Figure 7.

Classification accuracy obtained from mean of DEC and SEC. *X*-axis represents recursive cluster elimination steps in RCE-SVM algorithm. Olive Green line: classification accuracy obtained by using mean of DEC. Orange line: classification accuracy obtained using SEC. The number pairs above/below each knot denote the number of feature-clusters remaining (first number) and the number of features remaining (second number) at every cluster elimination step. Numbers in circles represent the *p*-value obtained by doing a two-sided *t*-test comparing classification accuracy obtained by mean of DEC with SEC (alternative hypothesis: accuracy using mean of DEC ≠ SEC) at every cluster elimination step. The error bars indicate the standard deviation in classification accuracy. [Color figure can be viewed at wileyonlinelibrary.com]

range of frequencies is higher for controls than PTSD subjects.

The features which both have significant group differences and are responsible for resulting in the highest accuracy were ascertained and displayed as a network of interconnected nodes using BrainNet Viewer visualization toolbox (http://www.nitrc.org/projects/bnv/) as shown in Figure 10. Here, the DFC obtained using a time-varying adaptive window length was used. The nodes represent centroids of brain regions, and each path represents each individual feature. The labels for the nodes in Figure 10 correspond to the names of corresponding ROIs (region of interest) derived from the AAL atlas (please refer to the tables in the Supporting Information S3 for MNI coordinates and AAL labels of all regions in the CC200 atlas). Paths with arrows denote EC, while paths without arrows denote FC. Further, the width and color of the paths correspond to their weights, which were calculated based on their SVM scores. Specifically, the SVM scores denote the importance of the corresponding feature for classification between the two groups [Craddock et al., 2009].

From Figure 10, a pattern emerges wherein PTSD subjects have stronger overall connectivity, but reduced temporal variability as compared to healthy controls. Specifically, we observed substantially less number of DEC and DFC paths whose variances were larger in PTSD subjects as compared to healthy controls than the other way around (Fig. 10A,B,E). Conversely, we observed substantially more number of SEC and SFC paths whose connectivity strength were larger in PTSD subjects as compared to healthy controls than the other way around (Fig. 10C,D,F). Note that no significant DFC paths were observed whose variances were larger in PTSD subjects as compared to healthy controls and at the same time had the discriminatory power to classify subjects with highest accuracy. Also, no significant SFC paths were observed whose connectivities were stronger in healthy controls as compared to PTSD and simultaneously had the discriminatory power to classify subjects with highest accuracy.

Apart from the general pattern mentioned above, there are specific patterns in each subfigure of Figure 10 which are noteworthy. First, it can be seen that both static and dynamic connectivity in cortico-cerebellar pathways are implicated in almost all subfigures of Figure 10, with predominantly increased static connectivity and decreased temporal variability in PTSD. Mid prefrontal cortex, precentral and postcentral cortices, caudate, and insula are also associated with increased static connectivity with

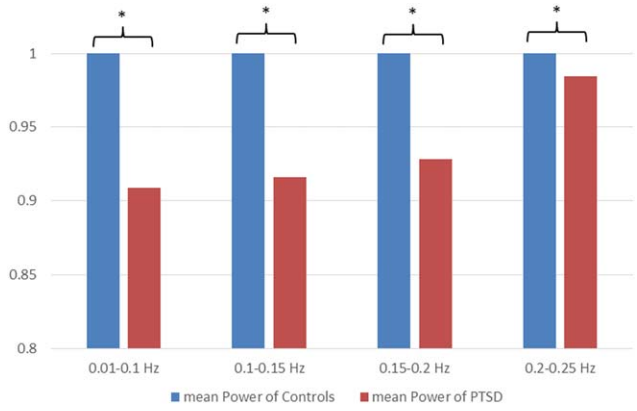

Figure 8.

Power Spectrum density plot of DFC for Controls and PTSD patients. The frequency range of 0.01 to 0.25 Hz is divided into four bins. The power for each frequency bin is normalized such that the power for Controls is 1. The blue bar represents power of Controls and the red bar represents power of PTSD. The * symbol indicates statistical significance. [Color figure can be viewed at wileyonlinelibrary.com]

decreased variability of connectivity in PTSD. Inferior and medial temporal lobes emerge as important hubs with highly ranked paths associated with them in Figure 10B,C,D, indicating their important roles in altered causal brain networks underlying PTSD. Conversely, the brainstem has predominantly stronger SFC in the PTSD. The number of incoming and outgoing paths for each region in each subfigure of Figure 10 (or just the number of paths associated with a given region for FC measures) along

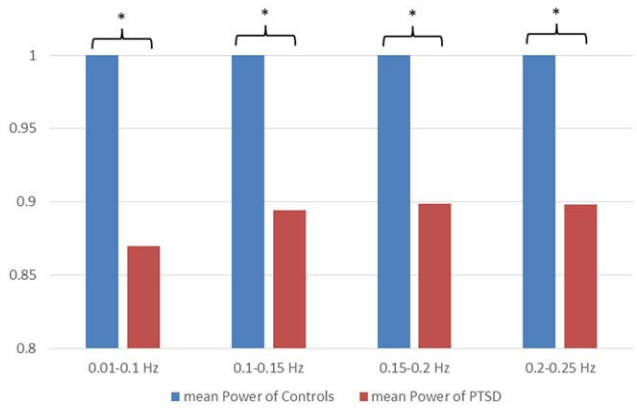

Figure 9.

Power Spectrum density plot of DEC for Controls and PTSD patients. The frequency range from 0.01 to 0.25 Hz is divided into four bins. The power for each frequency bin is normalized such that the power for Controls is 1. The blue bar represents power of Controls and the red bar represents power of PTSD. The * symbol indicates statistical significance. [Color figure can be viewed at wileyonlinelibrary.com]

with their summed connectivity weight is shown in Tables S1 and Table S2 of Supporting Information S3.

DISCUSSION

In this work, we tested the hypothesis that individuals with PTSD are characterized by reduced temporal variability of brain connectivity compared to healthy individuals, as inferred through resting-state fMRI. The motivation for this hypothesis stems from evidence in biological systems pointing to dynamic adaptability of function as a hallmark of health [Kleiger et al., 1987]. We specifically tested this hypothesis by predicting that in subjects diagnosed with PTSD, their brains will be characterized by elevated static connectivity (as shown in previous reports [Cisler et al., 2014]), coupled with decreased temporal variability of connections. Further, we investigated whether temporal variability of brain connectivity will provide increased sensitivity for predicting the diagnostic label of a novel subject, over and above the discriminatory power provided by conventional static connectivity.

The results presented in this article support the hypotheses stated above. Specifically, large number of DEC and DFC paths had variances which were significantly larger in healthy controls as compared to PTSD, in addition to providing impressive classification accuracies. In comparison, substantially less number of DEC paths, and no DFC paths, whose variances were larger in PTSD subjects as compared to healthy controls were observed at the end of RCE-SVM procedure. Conversely, large number of SEC and SFC paths whose connectivity strengths were higher in PTSD subjects as compared to healthy controls were observed. In comparison, substantially less number of SEC paths, and no SFC paths, whose connectivities were significantly stronger in healthy controls as compared to PTSD were observed. Taken together, these results support the notion that PTSD subjects have stronger overall connectivity, but reduced temporal variability of connectivity as compared to healthy controls. However, it should be noted that, since the dataset we used is limited to PTSD, future studies must examine whether this hypothesis holds true for other mental disorders.

Even though previous studies have demonstrated that dynamic connectivity signatures in healthy subjects are different from that in subjects diagnosed with mental diseases such as PTSD [Li et al., 2014] and schizophrenia [Sakoğlu et al., 2010], a key question has remained unanswered: whether dynamics of connectivity inferred from resting-state fMRI provides additional sensitivity to underlying causes of pathology or is it just a detailed characterization of conventional static connectivity with no additional predictive value. Our results support the hypotheses that dynamic connectivity indeed provides novel information as compared to static connectivity, which exhibits additional predictive value in clinical diagnosis. The classification results demonstrate that, at every iteration, including the one providing maximum

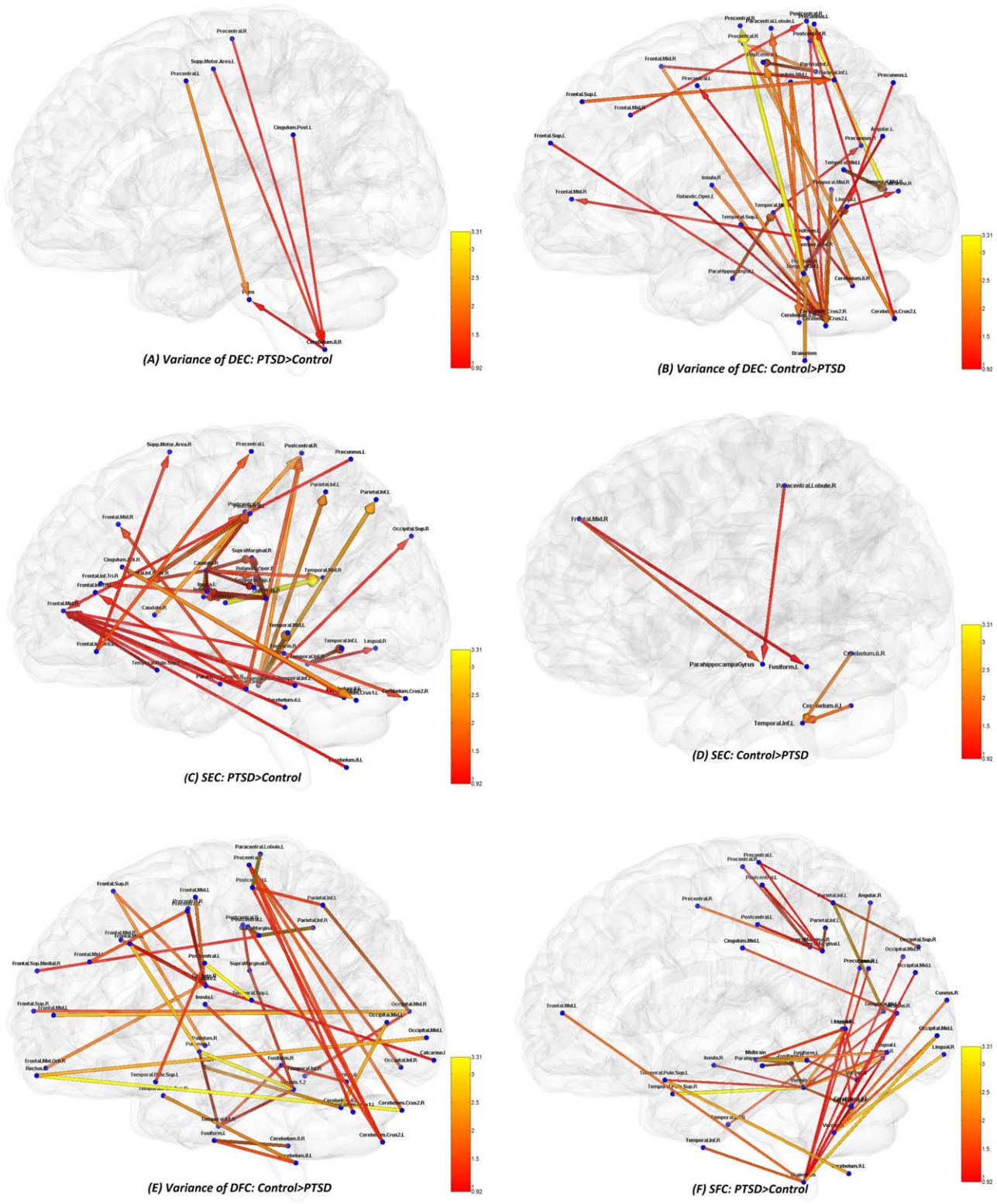
(A) Variance of DEC: PTSD>Control
(B) Variance of DEC: Control>PTSD
(C) SEC: PTSD>Control
(D) SEC: Control>PTSD
(E) Variance of DFC: Control>PTSD
(F) SFC: PTSD>Control

Figure 10.

accuracy, variance of DFC and DEC provided significantly higher classification accuracy than that provided by SFC and SEC. The fact that the maximum accuracy provided by variance of DFC and DEC exceeded 90% shows that it holds promise as a potential neuroimaging biomarker of PTSD.

PTSD is mainly associated with three symptom clusters: re-experiencing of the event and flashback, avoidance/numbing/depression, hyper-arousal, along with a high rate of dissociative symptoms [American Psychiatric Association, 1994; Yehuda, 2002]. Below we discuss some specific dynamic and static connectivity patterns (as in Fig. 10) that emerged from a statistical comparison between the groups in the context of the three symptom clusters mentioned above. Note that these paths (as shown in Fig. 10) were significantly different between the groups, as well as possessed the most predictive power (as ascertained through the SVM score) for determining the diagnostic label of a novel subject. First, both dynamic and static EC/FC paths associated with the cerebellum emerged as having significant differences between the two groups in Figure 10. As pointed out by Schmahmann and Pandya [1997], the cerebellum is engaged in the experience and regulation of emotions, especially fear perception, anxiety, anticipation, and recollection, and has afferent and efferent connections to the limbic system and brainstem [Wolf et al., 2009]. Thus, cerebellar function is known to be associated with PTSD symptom clusters [Baldacara et al., 2011; De Bellis and Kuchibhatla, 2006]. In addition, paths associated with the vermis region of the cerebellum were mainly implicated in FC differences between the groups. This region is believed to be functionally implicated with bodily posture and locomotion [Coffman et al., 2011], and has been shown to be associated with early traumatic life experiences [Baldacara et al., 2011].

Many EC paths associated with inferior and medial temporal lobes were significantly different between the two groups. Previous studies have shown that inferior and medial temporal lobes are crucial in relaying information among frontal lobe, limbic areas, cerebellum, and visual cortex. For example, as discussed by Miyashita [Miyashita, 1993], the inferior temporal cortex is referred to as the link from visual cortices to the limbic system and frontal lobe, acting to bind object perception with memory [Baylis and Rolls, 1987]. Medial temporal lobe is known to be involved in memory encoding and retrieval [Dove et al., 2006]. Since PTSD symptoms such as flashback and event re-experiencing are associated with memory systems, connectivity alterations in these regions are in line with previous research implicating them in PTSD [Qin et al., 2012].

The precentral and postcentral cortices, which contain the primary motor cortex and primary somatosensory cortex, respectively, had many associated EC and FC (both static and dynamic) paths which were different between PTSD and controls. In association with mid and inferior temporal cortices (these regions are connected to postcentral gyrus in Fig. 10B,C), postcentral gyrus has been previously implicated in emotion recognition, especially in social anxiety disorder [Hattingh et al., 2012; Lindemer et al., 2013], which relates to PTSD symptoms of numbing and depression. The precentral gyrus has been shown to be activated with the contrast of flashbacks versus ordinary episodic trauma memories in PTSD, as shown by Whalley et al. [2013].

Additional recruited areas for this contrast were sensory and motor areas including the insula, supplementary motor area (SMA), and mid-occipital cortex, as well as decreased connectivity in areas such as the midbrain, parahippocampal gyrus, and precuneus/posterior cingulate cortex. These regions were indeed involved in the significant differentiation between the two groups as in Figure 10: mid brain in Figure 10F; mid-occipital cortex reflected in FC subfigures; precuneus in Figure 10B,C,F; parahippocampal gyrus in Figure 10B–D,F; SMA in Figure 10A,C; insula in Figure 10B,C,E,F. The brain stem had many SFC connections to occipital and precuneus regions, as well as a path to the mid frontal cortex and a path to inferior temporal cortex, which were stronger in PTSD as compared to controls. The

Static and Dynamic connectivity features responsible for providing maximum classification accuracy between PTSD and healthy control groups. (A) Top ranked paths whose variances of DEC over time for PTSD subjects were significantly greater than those for healthy controls ($P < 0.05$). (B) Top ranked paths whose variances of DEC over time for healthy controls were significantly greater than those for PTSD subjects ($P < 0.05$). (C) Top ranked SEC paths which were significantly ($P < 0.05$) stronger in PTSD subjects as compared to healthy controls. (D) Top ranked SEC paths which were significantly ($P < 0.05$) stronger in healthy controls as compared to PTSD subjects. (E) Top ranked paths whose variances of DFC over time for healthy controls were significantly greater than those for PTSD subjects ($P < 0.05$). (F) Top ranked SFC paths which were significantly ($P < 0.05$) stronger in PTSD subjects as compared to healthy controls. DFC and SFC Paths have no arrows since correlation has no directionality. Note that no significant DFC paths were observed whose variances were larger in PTSD subjects as compared to healthy controls and at the same time had the discriminatory power to classify subjects with highest accuracy. Also, no significant SFC paths were observed whose connectivities were stronger in healthy controls as compared to PTSD and at the same time had the discriminatory power to classify subjects with highest accuracy. Therefore, no subfigures are displayed for them. In all subfigures, blue nodes represent centroids of functionally homogeneous CC200 brain regions, and paths with arrows connecting nodes represent EC metrics, whereas those without arrows represent FC metrics. The thickness and color of paths correspond to their weights (SVM score) calculated from RCE-SVM. Autumn color map is used with red representing low SVM score/rank and yellow representing high SVM score/rank. [Color figure can be viewed at wileyonlinelibrary.com]

brain stem has been previously implicated in various PTSD symptom clusters [Kemp et al., 2009; Moores et al., 2008]. However, this feature was not as discriminative as DFC differences between the groups. Other regions with multiple paths showing group differences, and which have been previously shown to be important regions underlying the pathophysiology of PTSD, were the caudate and insula [Herringa et al., 2012], parietal and occipital cortex [Whalley et al., 2013], fusiform [Shaw et al., 2009], and thalamus [Yin et al., 2011]. Among them, the insular cortex deserves to be highlighted since it is closely associated with pain and emotion, and an increasing number of neuroimaging studies show that both physical pain and depression involve the insular cortex [Fusar-Poli et al., 2009; Mutschler et al., 2012; Strigo et al., 2013]. The activation of fusiform has been shown by Shaw et al. [2009] to be linked to hyper-arousal and abnormal reactivity in PTSD. Besides, the parietal cortex is involved in the dorsal visual stream which appears to be altered in PTSD as compared to healthy controls [Whalley et al., 2013].

A question might arise as to whether PTSD subjects are actually mentally perseverating on traumatic memories in the scanner in resting-state, which could explain higher strength and lower variance in connectivity. The resting-state is a default baseline state of the brain, and responses during a particular task or a real-world scenario emerge out of this baseline state [Power et al., 2014]. Hence, if individuals with PTSD were to get entangled in heightened behaviors in real-world settings or experimental tasks, their brain networks responsible for such behaviors typically must already be "primed" for it during their baseline resting-state. Though it is not possible to comment on whether the PTSD subjects were consciously perseverating on the trauma in the scanner in resting-state, it can be said that conscious perseveration in resting-state is not a prerequisite to obtain hyper-connected networks which are less variable over time. Such hyper-connected and less-variable networks might define the subconscious baseline in resting-state, which might enable the emergence of heightened behaviors in PTSD subjects in real-world scenarios or experimental tasks.

This article presents some methodological advances which are noteworthy. First, few studies in the past have simultaneously examined both SFC and SEC from resting-state fMRI [Deshpande et al., 2011]. None have done so using both DFC and DEC in addition to conventional static metrics. We have studied and compared static as well as dynamic functional and effectivity connectivity. Second, most previous studies limit the number of ROIs either because they are using a seed-based approach [Yin et al., 2011] or because including more ROIs in EC models make them computationally intractable [Lohmann et al., 2012]. Exceptions to this include whole brain FC studies employing PCA [Viviani et al., 2005], ICA [van de Ven et al., 2004] and graph-theoretic approaches [van den Heuvel et al., 2008a, 2008b] and a limited number of whole brain EC studies employing conditional Granger causality [Wu et al., 2013]. None so far have simultaneously examined both FC and EC at the whole brain level, and our approach demonstrates a framework for doing so. Third, prior studies have used anatomically defined ROIs (e.g., from the AAL atlas [Leonardi et al., 2013], which make ROIs functionally heterogeneous) or have considered ROIs from pre-defined networks such as the default mode network [Qin et al., 2012]. Contrary to previous approaches, we have used functionally homogeneous ROIs obtained from spectral clustering of resting-state fMRI data (the CC200 atlas [Craddock et al., 2012]). This allowed us to perform whole brain analysis without adopting a voxel-wise approach (and hence avoiding computational intractability issues), and at the same time respect functional boundaries in the brain in ROI definition. Although the use of the CC200 functional atlas is not a novel methodological contribution (as it has been used before), we consider that it provides distinct advantages while performing whole brain analysis when voxel-wise analysis is computationally difficult to perform. Fourth, previous dynamic FC studies have used fixed-length sliding windows of arbitrary length. However, as noted before, different choices of window lengths would produce different smoothing effects [Chang and Glover, 2010; Leonardi et al., 2013], and since there is no data to suggest that the minimum length of the window within which the resting-state fMRI data is stationary, is constant over time, we relaxed the restriction of fixed window length and used time-varying window lengths instead. The principle we adopted is that the window length used must be the minimum length at which the time series become stationary, so that FC can be calculated over a period when the time series are stationary. The minimum window length condition allows us to capture maximum available dynamics. Our results indicate that using the time-varying window length for DFC calculation indeed improves the classification accuracy over the fixed window length DFC approach, thereby suggesting that variable window length DFC is more sensitive to fluctuations in functional connectivity and associated pathological changes. Similarly, for dynamic EC calculation, adapting the Kalman filter-based approach [Arnold et al., 1998] and calculating the forgetting factor (which controls the smoothness and hence is analogous to windows used in DFC calculation) made the parameter choices objective and hence the results reproducible. These proposed windowing strategies provide a principled approach for controlling the smoothness of estimated dynamic connectivity while respecting nonstationarity in the data. Finally, even though recent works have shown that dynamic connectivity signatures in healthy subjects are different from that in subjects diagnosed with mental diseases such as PTSD [Li et al., 2014] and schizophrenia [Sakoğlu et al., 2010], they do not answer the key question of whether dynamic connectivity provides any additional sensitivity to underlying neuronal processes than what is provided by conventional static connectivity. We have proposed a framework for answering this key question using a machine

learning-based approach called RCE-SVM, which can determine the predictive values of metrics derived from neuroimaging for diagnosis. This allowed us to investigate whether the dynamic connectivity patterns found to be statistically different between the groups provided any additional information than their static counterparts.

REFERENCES

Arnold M, Miltner WHR, Witte H, Bauer R, Braun C (1998): Adaptive AR modeling of nonstationary time series by means of kalman filtering. IEEE Trans Biomed Eng 45:553–562.

American Psychiatric Association (1994): Diagnostic and Statistical Manual of Mental Disorders (DSM IV), 4th ed. Washington, DC: American Psychiatric Association.

Baldacara L, Jackowski AP, Schoedl A, Pupo M, Andreoli SB, Mello MF, Lacerda AL, Mari JJ, Bressan RA (2011): Reduced cerebellar left hemisphere and vermal volume in adults with PTSD from a community sample. J Psychiatr Res 45:1627–1633.

Bassett DS, Wymbs NF, Porter MA, Mucha PJ, Carlson JM, Grafton ST (2011): Dynamic reconfiguration of human brain networks during learning. Proc Natl Acad Sci USA 108: 7641–7646.

Baylis GC, Rolls ET (1987): Responses of neurons in the inferior temporal cortex in short term and serial recognition memory tasks. Exp Brain Res 65:614–622.

Bressler SL, Seth AK (2011): Wiener-Granger Causality: A well established methodology. NeuroImage 58:323–329.

Britz J, Van De Ville D, Michel CM (2010): BOLD correlates of EEG topography reveal rapid resting-state network dynamics. Neuroimage 52:1162–1170.

Chang C, Glover GH (2010): Time–frequency dynamics of resting-state brain connectivity measured with fMRI. NeuroImage 50: 81–98.

Chang C, Liu Z, Chen MC, Liu X Duyn J (2013a): EEG correlates of time-varying BOLD functional connectivity. NeuroImage 72: 227–236.

Chang C, Metzger CD, Glover GH, Duyn JH, Heinze HJ, Walter M (2013b): Association between heart rate variability and fluctuations in resting-state functional connectivity. Neuroimage 68:93–104.

Cisler JM, Steele JS, Lenow JK, Smitherman S, Everett B, Messias E, Kilts CD (2014): Functional reorganization of neural networks during repeated exposure to the traumatic memory in posttraumatic stress disorder: An exploratory fMRI study. J Psychiatr Res 48:47–55.

Coffman KA, Dum RP, Strick PL (2011): Cerebellar vermis is a target of projections from the motor areas in the cerebral cortex. Proc Natl Acad Sci USA 108:16068–16073.

Craddock R, Holtzheimer P, Hu X, Mayberg H (2009): Disease state prediction from resting state functional connectivity. Magn Reson Med 62:1619–1628.

Craddock RC, James GA, Holtzheimer PE, Hu X, Mayberg HS (2012): A whole brain fMRI atlas generated via spatially constrained spectral clustering. Hum Brain Mapp 33:1914–1928.

Cribben I, Haraldsdottir R, Atlas LY, Wager TD, Lindquist MA (2012): Dynamic connectivity regression: Determining state-related changes in brain connectivity. Neuroimage 61:907–920.

De Bellis MD, Kuchibhatla M (2006): Cerebellar volumes in pediatric maltreatment-related posttraumatic stress disorder. Biol Psychiatry 60:697–703.

Deshpande G, Hu X (2012): Investigating effective brain connectivity from fMRI data: Past findings and current issues with reference to granger causality analysis. Brain Connect 2:235–245.

Deshpande G, LaConte S, Peltier S, Hu X (2006): Connectivity analysis of human functional MRI data:from linear to nonlinear and static to dynamic. Lecture Notes Comput Sci 4091:17–24.

Deshpande G, Hu X, Stilla R, Sathian K (2008): Effective connectivity during haptic perception: A study using Granger causality analysis of functional magnetic resonance imaging data. NeuroImage 40:1807–1814.

Deshpande G, LaConte S, James GA, Peltier S, Hu X (2009): Multivariate Granger causality analysis of brain networks. Hum Brain Mapp 30:1361–1373.

Deshpande G, Hu X, Lacey S, Stilla R, Sathian K (2010a): Object familiarity modulates effective connectivity during haptic shape perception. NeuroImage 49:1991–2000.

Deshpande G, Sathian K, Xiaoping H (2010b): Assessing and compensating for zero-lag correlation effects in time-lagged granger causality analysis of fMRI. IEEE Trans Biomed Eng 57: 1446–1456.

Deshpande G, Li Z, Santhanam P, Lynch CD, Coles ME, Hamann S, Hu X (2010c): Recursive cluster elimination based support vector machine for disease state prediction using resting state functional and effective brain connectivity. PLoS One 5:e14277.

Deshpande G, Santhanam P, Hu X (2011): Instantaneous and causal connectivity in resting state brain networks derived from functional MRI data. NeuroImage 54:1043–1052.

Deshpande G, Libero L, Sreenivasan KR, Deshpande H, Kana RK (2013): Identification of neural connectivity signatures of autism using machine learning. Front Hum Neurosci 7:670.

Dickey DA, Fuller WA (1979): Distribution of the estimators for autoregressive time series with a unit root. J Am Stat Assoc 74: 427–431.

Dimitriadis SI, Laskaris NA, Tsirka V, Vourkas M, Micheloyannis S (2012): An EEG study of brain connectivity dynamics at the resting state. Nonlinear Dynamics, Psychol life Sci 16:5–22.

Dove A, Brett M, Cusack R, Owen AM (2006): Dissociable contributions of the mid-ventrolateral frontal cortex and the medial temporal lobe system to human memory. NeuroImage 31:1790–1801.

Feng C, Deshpande G, Liu C, Gu R, Luo Y-J, Krueger F (2015): Diffusion of responsibility attenuates altruistic punishment: A functional magnetic resonance imaging effective connectivity study. Hum Brain Mapp 37:663–677.

Friston K (1994): Functional and effective connectivity in neuroimaging: A synthesis. Hum Brain Mapp 2:56–78.

Friston KJ, Frith CD, Liddle PF, Frackowiak RS (1993): Functional connectivity: The principal-component analysis of large (PET) data sets. J Cereb Blood Flow Metab 13:5–14.

Friston KJ, Harrison L, Penny W (2003): Dynamic causal modeling. NeuroImage 19:1273–1302.

Fusar-Poli P, Placentino A, Carletti F, Landi P, Allen P, Surguladze S, Benedetti F, Abbamonte M, Gasparotti R, Barale F, Perez J, McGuire P, Politi P (2009): Functional atlas of emotional faces processing: A voxel-based meta-analysis of 105 functional magnetic resonance imaging studies. J Psychiatry Neurosci 34:418–432.

Geweke J (1982): Measurement of linear dependence and feedback between multiple time series. J Am Stat Assoc 77:304–313.

Granger CWJ (1969): Investigating causal relations by econometric models and cross-spectral methods. Econometrica 37:424–438.

Grant MM, White D, Hadley J, Hutcheson N, Shelton R, Sreenivasan K, Deshpande G (2014): Early life trauma and

directional brain connectivity within major depression. Hum Brain Mapp 35:4815–4826.
Grant MM, Wood K, Sreenivasan KR, Wheelock M, White D, Thomas J, Knight DC, Deshpande G (2015): Influence of early life stress on intra- and extra-amygdaloid causal connectivity. Neuropsychopharmacology 40:1782–1793.
Greicius MD, Supekar K, Menon V, Dougherty RF (2009): Resting-state functional connectivity reflects structural connectivity in the default mode network. Cereb Cortex 19:72–78.
Greiser KH, Kluttig A, Schumann B, Swenne CA, Kors JA, Kuss O, Haerting J, Schmidt H, Thiery J, Werdan K (2009): Cardiovascular diseases, risk factors and short-term heart rate variability in an elderly general population: The CARLA study 2002–2006. Eur J Epidemiol 24:123–142.
Guye M, Bettus G, Bartolomei F, Cozzone PJ (2010): Graph theoretical analysis of structural and functional connectivity MRI in normal and pathological brain networks. MAGMA 23:409–421.
Hampstead BM, Stringer AY, Stilla RF, Deshpande G, Hu X, Moore AB, Sathian K (2011): Activation and effective connectivity changes following explicit-memory training for face-name pairs in patients with mild cognitive impairment. A pilot study. Neurorehabil Neural Repair 25:210–222.
Hampstead BM, Khoshnoodi M, Yan W, Deshpande G, Sathian K (2016): Patterns of effective connectivity during memory encoding and retrieval differ between patients with mild cognitive impairment and healthy older adults. NeuroImage 124: 997–1008.
Handwerker DA, Roopchansingh V, Gonzalez-Castillo J, Bandettini PA (2012): Periodic changes in fMRI connectivity. NeuroImage 63:1712–1719.
Hattingh CJ, Ipser J, Tromp SA, Syal S, Lochner C, Brooks SJ, Stein DJ (2012): Functional magnetic resonance imaging during emotion recognition in social anxiety disorder: An activation likelihood meta-analysis. Front Hum Neurosci 6:347.
Havlicek M, Jan J, Milan B, Calhoun VD (2010): Dynamic Granger causality based on Kalman filter for evaluation of functional network connectivity in fMRI data. NeuroImage 53:65–77.
Hayes JP, Vanelzakker MB, Shin LM (2012): Emotion and cognition interactions in PTSD: A review of neurocognitive and neuroimaging studies. Front Integr Neurosci 6:89.
Herringa R, Phillips M, Almeida J, Insana S, Germain A (2012): Post-traumatic stress symptoms correlate with smaller subgenual cingulate, caudate, and insula volumes in unmedicated combat veterans. Psychiatry Res 203:139–145.
Hillary FG, Roman CA, Venkatesan U, Rajtmajer SM, Bajo R, Castellanos ND (2015): Hyperconnectivity is a fundamental response to neurological disruption. Neuropsychology 29:59–75.
Hutcheson NL, Sreenivasan KR, Deshpande G, Reid MA, Hadley J, White DM, Ver Hoef L, Lahti AC (2015): Effective connectivity during episodic memory retrieval in schizophrenia participants before and after antipsychotic medication. Hum Brain Mapp 36:1442–1457.
Hutchison RM, Womelsdorf T, Gati JS, Everling S, Menon RS (2012): Resting-state networks show dynamic functional connectivity in awake humans and anesthetized macaques. Hum Brain Mapp 34:2154–2177.
Hutchison RM, Womelsdorf T, Allen EA, Bandettini PA, Calhoun VD, Corbetta M, Della PS, Duyn JH, Glover GH, Gonzalez-Castillo J, Handwerker DA, Keilholz S, Kiviniemi V, Leopold DA, de Pasquale F, Sporns O, Walter M, Chang C (2013): Dynamic functional connectivity: Promise, issues, and interpretations. Neuroimage 80:360–378.
Inza I, Larranaga P, Blanco R Cerrolaza AJ (2004): Filter versus wrapper gene selection approches in DNA microarray domains. Artif Intell Med 31:91–103.
Jatzko A, Schmitt A, Demirakca T, Weimer E, Braus DF (2006): Disturbance in the neural circuitry underlying positive emotional processing in post-traumatic stress disorder (PTSD). An fMRI study. Eur Arch Psychiatry Clin Neurosci 256:112–114.
Jia H, Hu X, Deshpande G (2014): Behavioral relevance of the dynamics of the functional brain connectome. Brain Connect 4: 741–759.
Kaminski M, Ding M, Truccolo WA, Bressler SL (2001): Evaluating causal relations in neural systems: Granger causality, directed transfer function and statistical assessment of significance. Biol Cybern 85:145–157.
Kapogiannis D, Deshpande G, Krueger F, Thornburg MP, Grafman JH (2014): Brain networks shaping religious belief. Brain Connect 4:70–79.
Keilholz SD, Magnuson ME, Pan WJ, Willis M, Thompson GJ (2013): Dynamic properties of functional connectivity in the rodent. Brain Connect 3:31–40.
Kemp AH, Felmingham KL, Falconer E, Liddell BJ, Bryant RA, Williams LM (2009): Heterogeneity of non-conscious fear perception in posttraumatic stress disorder as a function of physiological arousal: An fMRI study. Psychiatry Res 174:158–161.
Kleiger RE, Miller JP, Bigger JT, Moss AJ (1987): Decreased heart rate variability and its association with increased mortality after acute myocardial infarction. Am J Cadiol 59:256–262.
Kriegeskorte N, Simmons W, Bellgowan P, Baker C (2009): Circular analysis in systems neuroscience: The dangers of double dipping. Nat Neurosci 12:535–540.
Krueger F, Landgraf S, van der Meer E, Deshpande G, Hu X (2011): Effective connectivity of the multiplication network: A functional MRI and multivariate Granger Causality Mapping study. Hum Brain Mapp 32:1419–1431.
Lacey S, Hagtvedt H, Patrick VM, Anderson A, Stilla R, Deshpande G, Hu X, Sato JR, Reddy S, Sathian K (2011): Art for reward's sake: Visual art recruits the ventral striatum. NeuroImage 55:420–433.
Lee HL, Zahneisen B, Hugger T, LeVan P, Hennig J (2013): Tracking dynamic resting-state networks at higher frequencies using MR-encephalography. NeuroImage 65:216–222.
Leonardi N, Richiardi J, Gschwind M, Simioni S, Annoni JM, Schluep M, Vuilleumier P, Van De Ville D (2013): Principal components of functional connectivity: A new approach to study dynamic brain connectivity during rest. NeuroImage 83:937–950.
Li X, Zhu D, Jiang X, Jin C, Zhang X, Guo L, Zhang J, Hu X, Li L, Liu T (2014): Dynamic functional connectomics signatures for characterization and differentiation of PTSD patients. Hum Brain Mapp 35:1761–1778.
Liang P, Li Z, Deshpande G, Wang Z, Hu X, Li K (2014): Altered causal connectivity of resting state brain networks in amnesic MCI. PLoS One 9:e88476.
Libero LE, DeRamus TP, Lahti AC, Deshpande G, Kana RK (2015): Multimodal neuroimaging based classification of Autism Spectrum Disorder using anatomical, neurochemical and white matter correlates. Cortex 66:46–59.
Lindemer ER, Salat DH, Leritz EC, McGlinchey RE Milberg WP (2013): Reduced cortical thickness with increased lifetime burden of PTSD in OEF/OIF Veterans and the impact of comorbid TBI. Neuroimage 2:601–611.
Lohmann G, Erfurth K, Muller K,Turner R (2012): Critical comments on dynamic causal modelling. NeuroImage 59:2322–2329.

Majeed W, Magnuson M, Hasenkamp W, Schwar H, Schumacher EH, Barsalou L, Keilholz SD (2011): Spatiotemporal dynamics of low frequency BOLD fluctuations in rats and humans. NeuroImage 54:1140–1150.

McIntosh AR, Gozales-Lima F (1994): Structural equation modelling and its application to network analysis in functional brain imaging. Hum Brain Mapp 2:2–22.

Miyashita Y (1993): Inferior temporal cortex: Where visual perception meets memory. Annu Rev Neurosci 16:245–263.

Moores KA, Clark CR, McFarlane AC, Brown GC, Puce A Taylor DJ (2008): Abnormal recruitment of working memory updating networks during maintenance of trauma-neutral information in post-traumatic stress disorder. Psychiatry Res 163: 156–170.

Mutschler I, Ball T, Wankerl J, Strigo IA (2012): Pain and emotion in the insular cortex: Evidence for functional reorganization in major depression. Neurosci Lett 520:204–209.

Pan W (2002): A comparative review of statistical methods for discovering differentially expressed genes in replicated microarray experiments. Bioinformatics 546–554.

Patel RS, DuBois Bowman F, Rilling JK (2006): A Bayesian approach to determining connectivity of the human brain. Hum Brain Mapp 27:267–276.

Power JD, Schlaggar BL, Petersen SE (2014): Studying brain organization via spontaneous fMRI signal. Neuron 84:681–696.

Pruesse F, van der Meer E, Deshpande G, Krueger F, Wartenburger I (2011): Fluid intelligence allows flexible recruitment of the parieto-frontal network in analogical reasoning. Front Hum Neurosci 5:22.

Qin L, Wang Z, Sun Y, Wan J, Su S, Zhou Y, Xu J (2012): A preliminary study of alterations in default network connectivity in post-traumatic stress disorder patients following recent trauma. Brain Res 1484:50–56.

Roebroeck A, Formisano E, Goebel R (2005): Mapping directed influence over the brain using Granger causality and fMRI. NeuroImage 25:230–242.

Rogers BP, Katwald SB, Morgana VL, Gore CL, Asplunde JC (2010): Functional MRI and multivariate autoregressive models. Magn Reson Imaging 28:1058–1065.

Said SE, Dickey DA (1984): Testing for unit roots in autoregressive moving average models of unknown order. Biometrika 71: 599–607.

Sakoğlu U, Pearlson GD, Kiehl KA, Wang YM, Michael AM, Calhoun VD (2010): A method for evaluating dynamic functional network connectivity and task-modulation: Application to schizophrenia. MAGMA 23:351–366.

Sathian K, Lacey S, Stilla R, Gibson GO, Deshpande G, Hu X, LaConte S, Glielmi C (2011): Dual pathways for haptic and visual perception of spatial and texture information. NeuroImage 57:462–475.

Sathian K, Deshpande G, Stilla R (2013): Neural changes with tactile learning reflect decision level reweighting of perceptual readout. J Neurosci 33:5387–5398.

Sato JR, Junior EA, Takahashi Felix DY, de Maria M, Brammer MJ, Morettin PA (2006): A method to produce evolving functional connectivity maps during the course of an fMRI experiment using wavelet-based time-varying Granger causality. Neuroimage 31:187–196.

Schlogl A, Roberts SJ, Pfurtscheller G (2000): A criterion for adaptive autoregressive models. In: IEEE, editor. Proceedings of the 22nd IEEE International Conference on Engineering in Medicine and Biology. pp. 1581–1582.

Schmahmann JD, Pandya DN (1997): The cerebrocerebellar system. In: Schmahmann JD, editor. The Cerebellum and Cognition. San Diego, California: Academic Press. pp. 31–60.

Schwartz G (1978): Estimating the dimension of a model. Ann Stat 6:461–464.

Shaw ME, Moores KA, Clark RC, McFarlane AC, Strother SC, Bryant RA, Brown GC, Taylor JD (2009): Functional connectivity reveals inefficient working memory systems in post-traumatic stress disorder. Psychiatry Res 172:235–241.

Simmons AN, Matthews SC (2012): Neural circuitry of PTSD with or without mild traumatic brain injury: A meta-analysis. Neuropharmacology 62:598–606.

Stephan KE, Roebroeck A (2012): A short history of causal modeling of fMRI data. NeuroImage 62:856–863.

Stilla R, Deshpande G, Laconte S, Hu X Sathian K (2007): Posteromedial parietal cortical activity and inputs predict tactile spatial acuity. J Neurosci 27:11091–11102.

Stilla R, Hanna R, Mariola E, Deshpande G, Hu X, Sathian K (2008): Neural processing underlying tactile microspatial discrimination in the blind: A functional magnetic resonance imaging study. J Vis 8:13.1–19.

Strenziok M, Krueger F, Deshpande G, Lenroot RK, van der Meer E, Grafman J (2011): Fronto-parietal regulation of media violence exposure in adolescents: A multi-method study. Soc Cogn Affect Neurosci 6:537–547.

Strigo IA, Matthews SC, Simmons AN (2013): Decreased frontal regulation during pain anticipation in unmedicated subjects with major depressive disorder. Transl. Psychiatry 3:e239.

Tagliazucchi E, von Wegner F, Morzelewski A, Brodbeck V, Laufs H (2012): Dynamic BOLD functional connectivity in humans and its electrophysiological correlates. Front Hum Neurosci 6: 339.

Thompson GJ, Magnuson ME, Merritt MD, Schwarb H, Pan WJ, McKinley A, Tripp LD, Schumacher EH, Keilholz SD (2013): Short-time windows of correlation between large-scale functional brain networks predict vigilance intraindividually and interindividually. Hum Brain Mapp 34:3280–3298.

Valdes-Sosa PA, Roebroeck A, Friston J, Daunizeau K (2011): Effective connectivity: Influence, causality and biophysical modeling. NeuroImage 58:339–361.

van de Ven VG, Formisano E, Prvulovic D, Roeder CH, Linden DE (2004): Functional connectivity as revealed by spatial independent component analysis of fMRI measurements during rest. Hum Brain Mapp 22:165–178.

van den Heuvel M, Mandl R, Hulshoff Pol H (2008a): Normalized cut group clustering of resting-state FMRI data. PLoS One 3: e2001.

van den Heuvel MP, Stam CJ, Boersma Pol M, Hulshoff HE (2008b): Small-world and scale-free organization of voxel-based resting-state functional connectivity in the human brain. Neuroimage 43:528–539.

Vapnik VN (1995): The Nature of Statistical Learning Theory. New York: Springer.

Viviani R, Grön G, Spitzer M (2005): Functional principal component analysis of fMRI data. Hum Brain Mapp 24:109–129.

Wang L (2005): Support Vector Machines: Theory and Applications. New York: Springer.

Whalley MG, Kroes MCW, Huntley Z, Rugg MD, Davis SW, Brewin CR (2013): An fMRI investigation of posttraumatic flashbacks. Brain Cogn 81:151–159.

Wheelock MD, Sreenivasan KR, Wood KH, Ver Hoef LW, Deshpande G, Knight DC (2014): Threat-related learning relies

on distinct dorsal prefrontal cortex network connectivity. NeuroImage 102:904–912.

Wolf U, Rapoport MJ, Schweizer TA (2009): Evaluating the affective component of the cerebellar cognitive affective syndrome. J Neuropsychiatry Clin Neurosci 21:245–253.

Wu G, Stramaglia S, Chen H, Liao W, Marinazzo D (2013): Mapping the voxel-wise effective connectome in resting state fMRI. PLoS One 8:e73670.

Yan, C-G, Zang Y-F (2010): DPARSF: a MATLAB toolbox for "pipeline" data analysis of resting-state fMRI. Front Syst Neurosci 4:13.

Yehuda R (2002): Post-traumatic stress disorder. N Engl J Med 346:108–114.

Yin Y, Jin C, Hu X, Duan L, Li Z, Song M, Chen H, Feng B, Jiang T, Jin H, Wong C, Gong Q, Li L (2011): Altered resting-state functional connectivity of thalamus in earthquake-induced posttraumatic stress disorder: A functional magnetic resonance imaging study. Brain Res 1411:98–107.

Yin Y, Jin C, Eyler LT, Jin H, Hu X, Duan L, Zheng H, Feng B, Huang X, Shan B, Gong Q, Li L (2012): Altered regional homogeneity in post-traumatic stress disorder: A resting-state functional magnetic resonance imaging study. Neurosci Bull 28: 541–549.

Yousef M, Jung S, Showe LC, Showe MK (2007): Recursive Cluster Elimination (RCE) for classification and feature selection from gene expression data. BMC Bioinformatics 8:144.